A CFD ANALYSIS OF CONTROLLED FLUTTER PHENOMENON

by

Velmurugan THIRUSANGU [a*] ***and Parammasivam KANJIKOIL MAHALI*** [b]

[a] Department of Mechanical Engineering, University College of Engineering, Villupuram Tamil Nadu, India
[b] Department of Aerospace Engineering, Madras Institute of Technology, Anna University, Chennai, Tamil Nadu, India

Original scientific paper
DOI: 10.2298/TSCI16S4955T

In the present study, the concept of aero elastic wind energy generator is utilized wind turbines and it applied to produce electricity at low wind speeds. Flutter is the mechanism of dynamic instability in which the energy can be extracted from the wind. This energy might possibly transform into electric power. A straight rectangular wing with single degree of freedom at stalling angle is employed to do suitable work for producing power. A computational model of aero elastic wind energy generator is developed by using ICEM CFD and the flow analysis is carried out at different speeds for the prediction of co-efficient of power for the proposed device. Further a small model is experimentally fabricated and tested in a wind tunnel with different velocities using non-linear theory to predict the power co-efficient of a model. The test results from experiment are compared with the computational results. Thus it is evident that the correlated results are accurate within the acceptable range. The input from the flow analysis is used for structural analysis in ANSYS. The frequency, amplitude of oscillation and phase response of the proposed system can be obtained and it compared with the numerical values from MATLAB simulation of the same system to ensure for obtaining sustained oscillation which is capable of producing power. The flutter mechanism is having the advantage of producing power at very low velocity, eventhough low efficiency.

Key words: *renewable energy, torsional flutter, CFD, aero elasticity*

Introduction

Energy harvesting is a very attractive technique in recent decades and advances in energy harvesting from vibration that leads us to think of Aero elastic Wind Energy Generator (AeWEG). A model with base excitation of an elastically mounted seismic mass is developed. It has been reported that the efficiency of vibration based on energy harvest is proportional to the excitation frequency [1]. The maximum power flow for direct mass (force) and base excitation in the device depends on the vigor of the environment (frequency and amplitude of force) and the size of the device. The highly damped device yields less power [2]. So undamped natural frequency of the system is considered in developing the computational model. Flutter is an important aero elastic phenomenon in the field of aviation since its resulting motion is self-inducing and potentially excited oscillation which can interact or couple with the systems natural mode of vibration to cause

* Corresponding author; e-mail: velguru78@gmail.com

exhaustive damage [3]. However, the self-sustained oscillation of a NACA 0012 airfoil was witnessed during wind tunnel experiments [4]. Therefore, it appears that the aero elastic instability of flutter could be a method for converting wind energy into mechanical energy because of lot of energy got dissipated in the air surrounding the wing. A rigid airfoil with tensional degree of freedom can flutter only if the angle of attack is at or near the stalling angle [5]. The main problem is structural deformation caused by excitation due to the surface forces acted on the system. This can be solved by fluid-structure interaction [6]. Fluid-structure interaction (FSI) is the interaction where flow exerts pressure on a solid structure causing it to deform such that it perturbs the initial flow that is responsible for continuous self-excited oscillation. Aero elastic analysis is one special kind of FSI problem, of which interaction only performs on the interface of the fluid structure [7]. As flutter is self-excited oscillation, controlling factors are required to get sustained oscillation so that it can produce power [8]. The model will be analyzed and the systems power co-efficient is obtained to determine the maximum power that could be produced by the systematic different wind speeds and is validated with experimental results.

Modelling of fluid structure interaction

The physical model used in treating FSI phenomena vary enormously in their complexity and range of applicability. The simplest model is the very popular *piston theory*, which may be thought of as the limit of potential-flow models as the frequency of an oscillating body in a fluid becomes large [9]. It also may be thought of as the double limit as the Mach number becomes large, but the product of the Mach number and amplitude of oscillation normalized by body chord remains small compared with unity. This simplest theory expresses the fluid pressure, p, on the oscillating body at some point x, y, and sometime, t, as a simple linear function of the motion at that same point and instant in time. That is:

$$p \quad \frac{\rho U}{\mathrm{Ma}} \quad \frac{\partial w}{\partial t} \quad U\frac{\partial w}{\partial x} \tag{1}$$

where w is a function of x, y, and t and it is the instantaneous deflection of the body in the fluid stream, p, U, and Ma are the free-stream density, velocity, and Mach number, respectively. This simple fluid mechanics model has been very popular with structural engineering because it allows the fluid pressure to be incorporated into a standard structural dynamic with a minimum of additional complexity. But this fluid model is physically useful over only a limited range of flow conditions, and its primary value is in checking the results from more complex fluid models in the appropriate limit. There is a non-linear version of the piston theory, but it still is limited in the frequency or Mach number range where it is useful. Small-perturbation form of the potential-flow theory that leads to the celebrated linear convected wave equation for the velocity potential, Φ, that is:

$$\Phi \quad \frac{\mathrm{D}^2\Phi}{\mathrm{D}t^2} \quad 0 \tag{2}$$

where Φ is the Laplacian operation and D/Dt – the substantial derivative, which is, in turn:

$$\frac{\mathrm{D}}{\mathrm{D}t} \quad \frac{\partial}{\partial t} \quad U\frac{\partial}{\partial x} \tag{3}$$

The solution of the linear convected-wave equation forms the basis for many of the FSI models that have been used for FSI stability and response analyses of aircraft. These are termed *flutter* or *gust response* analyses.

Selection of model for aero elastic applications

Many approaches in computational aero elasticity seek to synthesize independent computational approaches for the aerodynamic and the structural dynamic subsystems. Some of the issues in coupling CFD and computational structural dynamics (CSD) are the former uses an Eulerian or spatially fixed co-ordinate system while the later uses a Lagrangian or material fixed co-ordinate subsystems. Hence, suitable interfacing technique should be used while performing coupling. Various interface methods like infinite plate spline, thin plate spline and multi quadratic biharmonic are used as an interfacing tool [10]. For every time step, one needs to map the surface loads from the CFD grid system onto the structural grid to obtain the forces on the CSD grid system, which are then used to obtain the displacements on the CSD grid and fig.1 shows the FSI flow diagram.

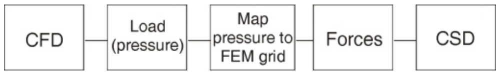

Figure 1. The FSI flow diagram

The computational challenge of FSI modelling

The FSI to obtain solution for many difference combinations of structural and fluid parameters, then to the CFD and other fluid models must be made as computationally efficient as possible [11]. For many years, in the analysis of complex structures, the finite element model (FEM) for a structural body undergoing oscillations has been reduced in size by first finding the natural or Eigen modes of the structure and then recasting the finite element structural model in terms of these modes, using, for example, Lagrange's equations from classical dynamics. A finite element structural model of a few thousand degrees of freedom (DOF) has been reduced to a nodal model with a few tens of DOF.

An oscillating aerofoil to demonstrate set-up and run a simulation involving two-way FSI in ANSYS Workbench. The transient structural analysis system and the fluid physics is set-up in fluid flow (CFX) analysis system, but both structural and fluid physics are solved together under the solution cell of the fluid system. Coupling between two analysis systems is required throughout the solution to model the interaction between structural and fluid systems as time progresses. The framework for the coupling is provided by the ANSYS multi-field solver using the MFX set-up. When ANSYS CFD-post reads an ANSYS results file, all the ANSYS variables are available to plot on the solid, including stresses and strains. The mesh regions available for plots by default are limited to the full boundary of the solid, plus certain named regions which are automatically created when particular types of load are added in simulation. For example, any fluid-solid interface will have a corresponding mesh region with a name such as FSIN 1.

Challenges in CFD/CSD coupling

In solving aero elastic problem, the first challenge is associated with computational cost of this simulation. However, the computational cost can be reduced via the implantation of parallel processing techniques, advanced algorithms, and improved computer hardware processing speeds. The 2nd one is the time taken for this computation. The CFD and CSD meshes do not match at the interface, CFD/CSD coupling requires a surface spline interpolation between the two domains. The interpolation of CSM modes shapes to CFD surface grid points is done as a pre-processing step. Modal deflections at all CFD surface grids are first generated. Modal data at these points are segmented based on the splitting of the flow field blocks. Mode shape deflection located at CFD surface grid points of each segment are used in the integration of the generalized modal forces and in the computation of the deflection at the deformed surface. The final surface deformation at each time step is a linear superposition of all modal deflections.

One reduced order model for aero elastic analysis using CFL3-D version was developed [12]. The aero elastic responses computed directly using the code is compared with the aero elastic responses computed with MATLAB environment which gives similar results.

Problem analysis

There are three variable in wing flutter [13]:
– flexure flutter,
– torsion flutter, and
– control surface rotation.

The rigid airfoil so constrained as to have only the flexural DOF does not flutter. A rigid airfoil with only the torsional DOF can flutter only if the angle of attack is at or near the stalling angle. So consider the oscillation of aileron control in the wing. That is control surface rotation of rigid aerofoil. Figure 2 shows the rigid, symmetric aerofoil restrained to rotate about is leading edge.

Consider only rigid wing with span, L_s. Rotates about leading edge with only torsional DOF does not have flexure flutter. Symmetric aerofoil NACA 0012, Chord length of the aerofoil 2b. Lift and moment of the wind is L and M.

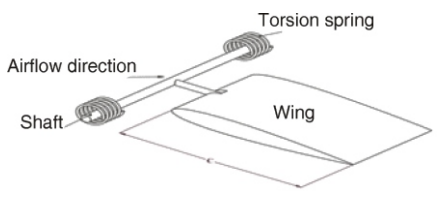

Figure 2. Rigid, symmetric aerofoil restrained to rotate about is leading edge

Derivation of equation of motion of the system [5]:

$$I_\alpha \frac{\mathrm{d}^2\alpha}{\mathrm{d}t^2} \quad k_\alpha \alpha \quad M_\mathrm{L} \tag{4}$$

Problem description

The NACA 0012, the well documented airfoil from the 4-digit series of NACA airfoils, is utilized. The NACA 0012 airfoil is symmetrical; the 00 indicates that it has no camber. The 12 indicates that the airfoil has a 12% thickness to chord length ratio; it is 12% as thick as it is long. Reynolds number for the simulations was Re = 3 10^6, same with the reliable experimental data from Abbott and Von Doenhoff [14], in order to validate the present simulation. The free stream temperature is 300 K, which is the same as the environmental temperature. The density of the air at the given temperature is ρ = 1.225 kg/m^3 and the viscosity is μ = 1.7894 10^{-5} kg/ms. The flow can be described as incompressible at this Reynolds number. This is an assumption close to reality and it is not necessary to resolve the energy equation. A segregated, implicit solver is utilized (ANSYS Fluent 6.3.26., 2006). Calculations was done for angles of attack ranging from –12 to 20°. The airfoil profile, boundary conditions, and meshes were all created in the pre-processor Gambit 2.4.6. The pre-processor is a program that can be employed to produce models in 2-D and 3-D, using structured or unstructured meshes, which can consist of a variety of elements, such as quadrilateral, triangular or tetrahedral elements. The resolution of the mesh was greater in regions where greater computational accuracy was needed, such as the region close to the airfoil.

Computational work

Although, early computational methods are an adaptation of the theoretical methods already in use, digital computing has led to the growing sophistication of aero elastic analyses. It is with the development of CSD and CFD that the possibility of the whole new avenues of aero elastic analysis opened. The coupling of the CFD models of various forms with CSD models in a simulation of a FSI is the origin called computational aero elasticity. While early methods employed simplified linear structural and fluid dynamic models, the rapid progress of computer technology in speed and memory has allowed continuous development of numerical models and opened the way for the new methods of simulation, design, and analysis. These in turn have led to significant strides in the understanding of aero elastic phenomena.

Computational grids

A CFD mesh is generated around the wing by placing the wing in the middle of the computational domain. The geometry could be generated by using the GAMBIT meshing software and ICEM CFD was used to construct the CFD mesh around the wing. It is a multi-block domain and C-grid was employed around the wing to preserve orthogonality of grid near the wing. Since it is very thin wing, care must be taken while generating mesh around the wingtip and trailing edge to avoid any negative cell volumes. Figure 3 shows the computational domain for 2-D

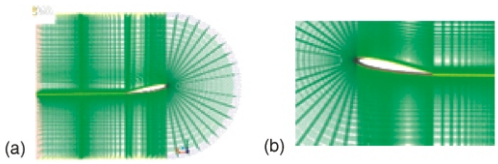

Figure 3. Computational domain for 2-D

Fluid flow solver

Navier-Strokes flow solver is considered as highly robust and accurate with excellent performance [15]. The code has been validated on a number of problems. Typically, algorithms for the Navier-Stokes equations can be broadly classified into either density or pressure-based methods. In both conditions, the velocity field is obtained via the momentum equations. The pressure is obtained via a pressure or a pressure correction equation, which is formulated by manipulating the continuity and momentum equations.

The solution procedure for pressure-based methods is typically sequential in nature, and if, can adapt to a varying number of equations without reformulating the entire algorithm. One of the algorithms that are originally developed for these pressure-based flow solvers is based on SIMPLE family of algorithms [10].

Typically, computations can be performed using either a staggered grid arrangement or a non-staggered or collocated grid arrangement. In the former arrangement, the velocities are stored at the cell face, rather than at the cell centers for the collocated arrangement. This makes the collocated grid system easier to use but it does require some interpolation procedure to evaluate the contravariant velocities at the cell faces. One such interpolation scheme devised is the momentum interpolation scheme. For unsteady computations, the interpolation procedure introduces the time step size factor into the formulation and there might be situations when one might be forced to use a small time step size based on the stability condition of the time marching procedure.

Code validation

One of the most important aspects of developing a computational tool is to validate the model with theory or prior computational results. Since there are many issues associated with a CAE model, code validation has been performed by looking each of the modules individually to ensure consistency with previously published results of these modules. First the CFD results will be shown, which will be followed by various issues. Then the results of the structural solver presented. Finally, results from the simplified structure model is compared with experimental results.

Structural analysis

Fluid-structure interaction

The interaction of the fluid and the structure at a mesh interface causes the acoustic pressure to exert a force applied to the structure and the structural motions produce an effective *fluid load*. The governing finite element matrix equations then become [16]:

$$[M_{\mathrm{s}}]\{U\} \quad [K_{\mathrm{s}}]\{u\} \quad \{F_{\mathrm{s}}\} \quad \{R\}[p] \tag{5}$$

$$[M_{\mathrm{f}}]\{P\} \quad [K_{\mathrm{f}}]\{p\} \quad \{F_{\mathrm{f}}\} \quad \rho[R]^{T}\{U\} \tag{6}$$

Here, $[R]$ is a coupling matrix that represents the effective surface area associated with each node on the FSI. The matrix $[R]$ also takes into account the direction of the normal vector defined for each pair of coincident fluid and structural element faces that comprises the interface surface. The positive direction of the normal vector, as the program uses it, is defined to be outward from the fluid mesh and in towards the structure. Both the structural and fluid load quantities that are produced at the FSI are functions of unknown nodal DOF. Placing these unknown *load* quantities on the left hand side of the equations and combining the two equations into a single equation produces the following [16]:

$$\begin{array}{cc} M_{\mathrm{s}} & O \\ \rho R^{T} & M_{\mathrm{f}} \end{array} \quad \begin{array}{c} U \\ P \end{array} \quad \begin{array}{cc} K_{\mathrm{s}} & R \\ O & K_{\mathrm{f}} \end{array} \quad \begin{array}{c} u \\ P \end{array} \quad \begin{array}{c} F_{\mathrm{s}} \\ F_{\mathrm{f}} \end{array} \tag{7}$$

The equation implies that nodes on a FSI have both displacement and pressure DOF.

Structure solver

The aim of this paper is to address the interaction of a complex fluid solver with a simplified structure solver, the structure solver is modelled using beam finite elements with only linear effects considered. This simplification allows for a good description of the motion of the wing, without being computationally hampered by complex non-linear effects. Since the wing is modelled as a linear structure, it is possible to model the deformations as a summation of different modes of deformation without looking at the complex interaction of the modes. The structure or the wing is modelled as a linear finite element structure that can undergo bending and torsion. The Bernoulli-Euler beam theory is enforced, which means the cross-sections remain rigid, thereby uncoupling the bending and torsional displacements. The linear finite element that, we choose to model the wing is a beam that has mass, stiffness, and damping matrices of the actual wing. Thus, the deformations become that of a Bernoulli-Euler beam bending and torsion, the equations for which reads [17]:

$$\frac{\mathrm{d}^2}{\mathrm{d}x^2} \quad EI\,\frac{\mathrm{d}^2 w}{\mathrm{d}x^2} \qquad f \tag{8}$$

where f is the distributed loading (force per unit length) acting in the same direction as the out-of-plane displacement w, E – the Young's modulus of the beam, and I – the area moment of inertia of the beam's cross-section. To find the equations of motion, Lagrange's equation is used. The equations take the form given by [17]:

$$\frac{\mathrm{d}}{\mathrm{d}t}\frac{\partial T}{\partial \dot{q}} \quad \frac{\partial T}{\partial q} \quad \frac{\partial V}{\partial q} \quad \frac{\partial F}{\partial \dot{q}} \quad Q \tag{9}$$

where q is the generalized displacements, vertical and torsional displacements, F – the Rayleigh dissipation function, and Q – the generalized forces. The kinetic energy and the potential energy of the wing are given by T and V, respectively.

The generalized co-ordinates for the wing are functions of the position of the cross section along the span of the wing and time. Here, the generalized co-ordinates are referred to as w, representing the classical generalized co-ordinates of bending, and y representing the classical generalized co-ordinates of torsion.

Structural analysis

In the ANSYS portion, the pitching motion of the airfoil is the only motion allowed and all other DOF are arrested [18]. The nodes of the surface mesh of ANSYS are same as that of the FLUENT portion using the shell 63 elements, so there is no problem in interpolating. Every analysis step restarts from the result of pre step. The material property is constant, isotropic and linear. Young's modulus is 2.9 10^9 N/m^2, Poisson's ratio is 0.1, and the density is 620 kg/m^3. Figure 4, shows the model for structural analysis and fig. 5 shows the airfoil model with support cylinder.

Figure 4. Model for structural analysis

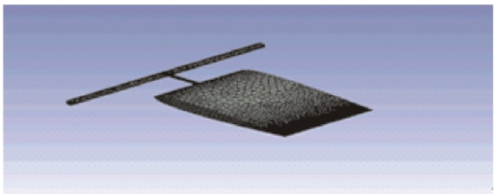

Figure 5. Airfoil model with support cylinder

Structural analysis is done by means of taking surfaces forces from CFD as loads on the FEM. It is considered as the shell type of problem since the surface forces are taken as nodal forces. The frequency and mode shape of the system are given in tab. 1, for first six foregoing modes and mode shapes shown in fig. 6.

Experimental work

The AeWEG fabrication

A prototype, scaled model with a scale ratio of 10 is fabricated [19]. It consists of a rectangular wing which wooden ribs connected by aluminum stringers and covered with polymer sheet to improve smoothness over the surface. The wing is connected to the shaft by welding. This shaft will rotate in a bearing and has a spring attached to the frame for suspending the wing at its stall angle of attack. Trailing edge of the wing has a bracket which connects the connecting rod to a crank at the bottom fixed to the frame. The set-up is a four bar linkage with the frame as the fourth and fixed link. The system has one DOF (s) since $s = 3(i - 1) - 2j = 1$. Where, number of joints (j) and number of links (i) are 4. Figure 6 shows the model of the AeWEG system.

Figure 6. Model of the AeWEG system

Table 1. Modes and frequency values

Modes	Frequency
1	0
2	0.25868E-01
3	0.96443E-01
4	0.41417
5	0.59452
6	1.3734

The fabricated scaled model (prototype) is kept at the rooftop of a 5-storey building resulting to the oscillation of the wing when the wind speeds exceeds 3 m/s. This oscillating motion is converted into rotary motion by the crank (mechanical work). This rotary motion may be converted into electrical energy by coupling a generator in the crankshaft. Weight of the connecting rod be kept minimum, as it should not be greater than the lift created by the wing. Steel is first preferred for the connecting rod and replaced by aluminum rods after realising that the lift must be greater than the weight of the rod. The crank produced 48 rpm at 10 m/s wind velocity. Power coefficient of the prototype is also found out at various velocities. Using eq. (10), power coefficient is calculated [20]:

$$C_P \quad \frac{1}{2} \quad 1 \quad \frac{V_2^2}{V_1^2} \quad \frac{V_2}{V_1} \tag{10}$$

For velocities 5, 10, and 15 m/s, it was observed that power co-efficient decreases with increase in velocity and the best operational velocity lies between 2 and 10 m/s. This fact is also proven from the wind tunnel tests that the velocity for oscillation lays within 10 m/s. After this velocity, the oscillations will reduce to insignificant values that the operation of the machine becomes unreasonable.

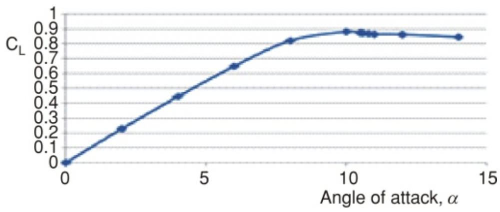

Figure 7. Variation between angle of attack and C_L at velocity 10 m/s

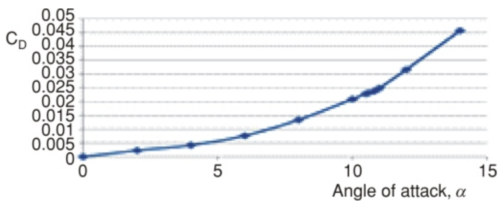

Figure 8. Variation between angle of attack and C_D at velocity 10 m/s

Results and discussions

Graphs are plotted with the help of C_L and C_D values for different angles of attack. These values are mainly used for calculating the surface forces and moments acting on the airfoil with given initial and boundary conditions, fig. 7.

An airfoil with stalling angle of attack produces flutter. It is observed, that pressure distribution around the aerofoil is varies with respect to angle of attack, fig. 8. Flutter initiate due to flow separation and vertox formation above stall angle of attack. So NACA 0012 airfoil with torsional stiffness at stallinf angle of attack is taken for analysis and the graphs and plots from the CFD analysis shows the occurance of flutter.

The airfoil at stalling angle produces vortices due to separation at the end or trailing edge. The variation of pressure at the trailing edge shows the production of vortices due to flutter at stalling angle, fig. 9.

The graph of velocity magnitude indicates the velocity on top and bottom surfaces for each station or position of the airfoil, fig. 10. The velocity at top surface is greater than the bottom surface at first then decreases and finally reaches the same velocity at the trailing edge.

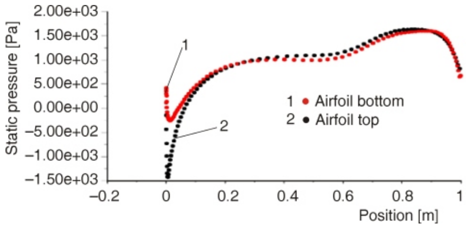

Figure 9. Variation of position with static pressure of flutter

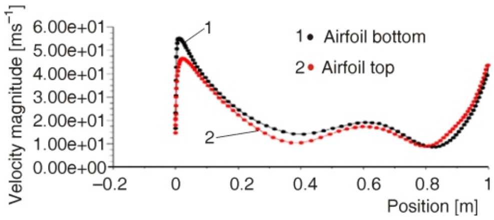

Figure 10. Variation of position with velocity magnitude of flutter

Figure 11 shous the static pressure contour for NACA 0012. The total pressure contour proves that the computed result is accurate because the pressure at bottom surface is higher than at the top, fig. 12.

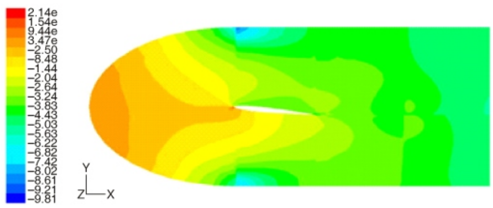

Figure 11. Static pressure contour for NACA 0012

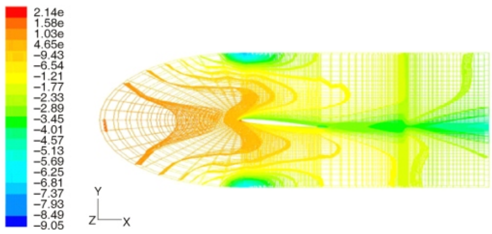

Figure 12. Total pressure contour for NACA 0012

Experimental validation

Correlation of C_p value from computational and experimental results

The coefficient of power is calculated for different velocities with the help of $V_1$and V_2 values taken from the computational results as well as experimental fabrication and the values are corelated in order to get a comparative data in figs. 13 and 14.

Numerical validation

The harmonic analysis obtained from ANSYS shows that the frequency of oscillation with constant amplitude which leads to sustained oscillation. The input for this analysis is taken

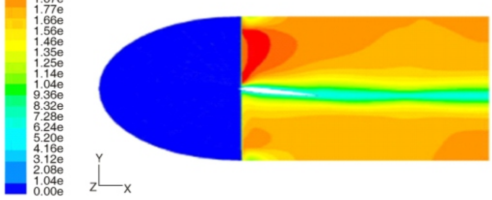

Figure 13. Velocity magnitude contour for NACA 0012

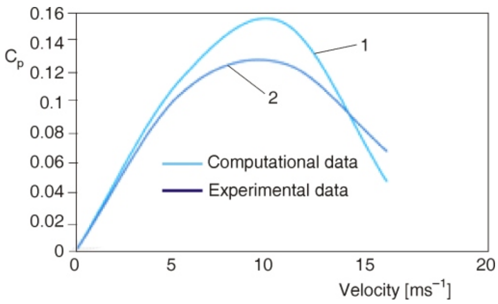

Figure 14. Velocity *vs.* power coefficicent

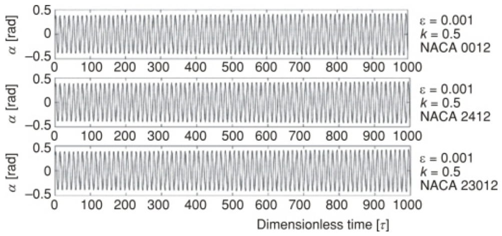

Figure 15. Evolution with dimensionless time of the amplitude of oscillation (rad) of AeWEG system (for different airfoil)

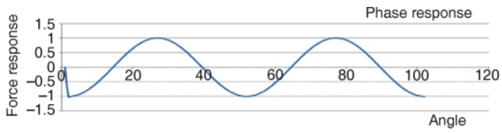

Figure16. Variation of output with respect to phase angle

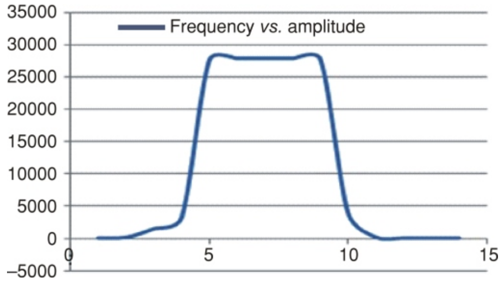

Figure 17. Frequeqncy *vs.* amplitude graph

from the modal analysis. The amplitude of oscillation obtained from numerical analysis is compared with the harmonic analysis results. The comparison of computational and numerical results shows that sustained oscillation required for power production is obtained.

Figures 15-17 clearly shows that the amplitude of oscillation is constant along certain frquency range. This constant amplitude with time per second will represent the sustained oscillation of the system.

Conclusion

The possibility of estimating the controlled or sustained oscillation range is analysed. The computational approach permits visualisation of the induced flow over the surface of the airfoil. The transient forces and moments acting on the airfoil and also the stiffness of the spring attached to the system are calculated with the help of CFD. The structural reaction of the system is calculated from analysis and the figuring and mode shapes are also calculated. The power coefficient is calculated at a velocity of 5 m/s. It has been found that the model becomes aero elastically unstable and torsional flutter begins at stalling angle. The maximum power output for a wind speed of 10 m/s is 0.169 W. Further when velocity at 15 m/s, the power co-efficient decreases and hence it is concluded that the viable velocity is 10 m/s for the flutter arrangement which has been proven through computationally. Further it has been concluded that the amplitude of oscillation is constant over a certain frequency range within which the required sustained oscillation. The optimisation of design parameters can be done in order to improve the efficiency of the proposed system.

Nomenclature

C_D – coefficient of drag
C_L – coefficient of lift
C_p – power coefficient
I_α – moment of inertia about the leading edge, [kgm^2]
k – reduced frequency
k_α – torsional stiffness of the spring, [Nmrad^{-1}]
K_s – structural stiffness matrix, [Nm^{-1}]
M_f – fluid mass matrix, [kg]
M_L – moment about leading edge of the aerofoil, [Nm]
M_s – structural mass matrix, [kg]
$\{U\}$ – acceleration, [rads^{-1}]
$\{u\}$ – displacement, [m]
$\{\ \}$ – force vector, [N]

Greek symbols

α – angle of restrained position of the wing, [rads^{-2}]
ε – dimensionless inertia
ρ – density, [kgm^{-3}]
Φ – velocity potential

Acronyms

DOF – degrees of freedom
NACA – National Advisory Committee for Aeronautics
CSM – computational structural modelling
CSD – computational structural dynamics
FEM – finite element model
FSI – fluid-structure interface

References

[1] Harb, A., Energy Harvesting: State of the Art, *J. Renewable Energy, 36* (2011), 10, pp. 2641-2654
[2] Stephen, N. G., On Energy Harvesting From Ambient Vibration, *J. Sound Vib., 293* (2006), 1-2, pp. 409-425
[3] Bisplinghoff, R. L., *et al.*, *Aero Elasticity*, Dover Publications Inc., Mineola, N. Y., USA, 1955
[4] Poirel, D., *et al.*, Self-Sustained Aero Elastic Oscillations of a Naca0012 Airfoil at Low-to-Moderate Reynolds Numbers, *J. Fluids Struct., 24* (2008), 5, pp. 700-719
[5] Fung, Y. C., *An Introduction to the Theory of Aero Elasticity*, Dover Publications, Mineola, N. Y., USA, 1969
[6] Wang, Y.-W., *et al.*, Combination of CFD & CSD Packages for Fluid Structure Interaction, *J. Hydrodyn, 20* (2008), 6, pp. 756-761
[7] Kamakoti, R., *et al.*, Fluid-Structure Interaction for Aero Elastic Applications, *Progress in Aerospace Sciences, 40* (2005), 8, pp. 535-598
[8] Caracoglia, L., Feasibility Assessment of a Leading-Edge-Flutter Wind Power Generator, *J. Wind Eng. Ind. Aerodyn.*; *98* (2010), 10-11, pp. 679-686
[9] Sharma, U., Effects Of Airfoil Geometry and Mechanical Characteristics on the on Set of Flutter, Ph. D. Thesis, Georgia Institute of Technology, Atlanta, Geo., USA, 2004
[10] Dang, H., *et al.*, Accelerated Loosely Coupled CFD/CSD method for Nonlinear Static Aeroelastic Analysis, *Aerospace Science and Technology, 14* (2010), 4, pp. 250-258
[11] Lee, B. H. K., *et al.*, Analysis and Computation of Nonlinear Dynamic Response of a Two-Degree-of Freedom System and its Application in Aero Elasticity, *J. Fluids Struct., 11* (1997), 3, pp. 225-246
[12] Silva, W. A., Bartels, R. E., Development of Reduced-Order Model for Aero Elastic Analysis and Flutter Prediction Using Cfl3dv6.0 Code, *Journal of Fluids and Structures, 19* (2009), 6, pp. 729-745
[13] Poirel, D., Yuan, W., Aerodynamics of Laminar Separation Flutter at a Transitional Reynolds Number, *J. Fluids Struct*., *26* (2010), 7-8, pp. 1174-1194
[14] Abbott, I. H., Von Doenhoff, A. E., Theory of Wing Sections. Dover Publications, Inc., Mineola, N. Y., USA, 1959
[15] Theodorsen, T., General Theory of Aerodynamic Instability and the Mechanism of Flutter, Report No. 496, NASA, Washington DC, 1935
[16] Goura, G. S. L., *et al.*, A Data Exchange Method for Fluid-Structure Interaction Problems, *Aeronautical Journal-New Series, 105* (2001), Apr., pp. 215-221
[17] Hoke, C. M., Comparison of Overset Grid and Grid Deformation Techniques Applied to 2-D Naca Airfoils, *Proceedings*, 19th AIAA Computational Fluid Dynamics Conference, San Antonio, Tex., USA, 2009
[18] Eleni, D. C., *et al.*, Evaluation of Turbulence Models for the Simulation of Flow Over a NACA 0012 Airfoil, *Journal of Mechanical Engineering Research, 4* (2012), 3, pp. 100-111
[19] Wang, D. A., *et al.*, Electromagnetic Energy Harvesting from Flow Induced Vibration, Microelectron, *Microelectron Journal, 41* (2010), 6, pp. 356-364
[20] Goodarz, A., Aeroelasticity Wind Energy Converter, *Journal of Energy Conversion, 18* (1978), 2, pp. 115-120

Paper submitted: September 12, 2015
Paper revised: January 7, 2016
Paper accepted: February 25, 2016